16th World Conference on Earthquake Engineering, 16WCEE 2017
Santiago Chile, January 9th to 13th 2017
Paper N° 4290
Registration Code: S-R1464636739

DEVELOPMENT OF A RECORD-BASED STOCHASTIC GROUND MOTION MODEL FOR CHILE

R. Silva[(1)], A.A. Taflanidis[(2)], G.P. Mavroeidis[(3)], C. Pastén[(4)]

[(1)] *Undergraduate Student, University of Chile, rodrigo.silva.l@ing.uchile.cl*
[(2)] *Associate Professor, University of Notre Dame, a.taflanidis@nd.edu*
[(3)] *Assistant Professor, University of Notre Dame, g.mavroeidis@nd.edu*
[(4)] *Assistant Professor, University of Chile, cpasten@ing.uchile.cl*

Abstract

Stochastic ground motion models can facilitate a versatile description of earthquake acceleration time histories by modulating a white-noise sequence through functions that address spectral and temporal properties of the excitation. This is established by (i) selecting appropriate time/frequency modulation functions and (ii) relating the parameters of these functions to seismological (fault type, moment magnitude and rupture distance) and site (shear wave velocity) characteristics through predictive relationships. Various approaches have been proposed to accomplish these tasks. Source-based models (also known as physics-based) rely on physical modeling of the rupture and wave propagation mechanisms, whereas record-based models (also known as site-based) are developed by fitting a preselected "waveform" to a suite of recorded regional ground motions. In recent years, record-based models have gained increasing popularity within the structural engineering community, due to their versatility in selecting their waveforms to capture all important features of ground motion (such as spectral non-stationarities, deemed important for inelastic structures). This paper investigates the development of a record-based stochastic ground motion model for Chile by utilizing a suite of ground motions recorded by the RENADIC (Red de cobertuta nacional de acelerografos) network and the Seismological Center of the University of Chile.

A stochastic model that addresses both temporal and spectral non-stationarities, corresponding to a series of cascading single-degree-of-freedom (SDOF) oscillators with time-varying frequency and damping, is adopted as the basis for this development. The stochastic model is then modified appropriately through information extracted from the available ground motion suite. This facilitates a complete parameterization of the time and frequency functions defining the stochastic ground motion model. An identification framework is then discussed that provides the optimal fit of the parameterized model to a specific ground motion, and a validation of the resultant model is proposed in terms of the corresponding response spectrum. The results of this identification are then exploited to develop, though regression analyses, predictive relationships that relate the model parameters to seismicity characteristics. This facilitates the generation of synthetic motions for specific seismic scenarios. The corresponding model and regression relationships are finally validated by comparison to regional ground motion prediction equations.

Keywords: ground motion; record-based stochastic model; regression analysis; subduction zone; Chile

1. Introduction

Seismic risk assessment requires description of the earthquake hazard through appropriate models that adequately address its variability for different seismicity levels. For applications involving dynamic analysis this description corresponds to the entire ground motion acceleration time history. The growing interest in the last decade in performance-based earthquake engineering (PBEE) [1] and in simulation-based mitigation approaches, especially for the design of high-performance protective devices such as floor and base-isolation systems and viscous dampers [2], has increased the importance of this task within the structural engineering community. In both instances, the need arises to address in detail the entire spectrum of response, ranging from linear to nonlinear to structural collapse, requiring a realistic, comprehensive characterization of earthquake acceleration time histories for a wide range of seismicity scenarios.

Undoubtedly the most popular approach for accomplishing this task for probabilistic seismic risk assessment is the scaling of ground motions based on Intensity Measures (IMs) for different hazard levels [3]. Though popular, this approach suffers from the fact [4] that the inherent variability of the acceleration time history is somewhat arbitrarily addressed by the exact selection of the ground motions. More importantly, scientific concerns exist regarding the validity of ground motion scaling, as it was shown that this approach may contribute to a significant bias in assessing seismic risk [5], especially when nonlinear behavior is of interest [6]. This realization has motivated researchers in the structural engineering field to put greater emphasis on stochastic ground motion models for characterizing seismic hazard [7]. These models are based on modulation of a stochastic sequence, through functions (filters) that address spectral and temporal characteristics of the excitation. The parameters of these filters are related to seismological (type of fault, moment magnitude and rupture distance) and site (shear wave velocity) characteristics through predictive relationships [7, 8]. This facilitates ultimately a comprehensive link to the resultant risk, established simply by adopting a probabilistic characterization for the seismological/site properties [9, 10].

The essential component of stochastic ground motion models is the development of the associated predictive relationships. *Source-based* models (also known as physics-based) [8, 11] rely on physical modeling of the rupture and wave propagation mechanisms, whereas *record-based* models (also known as site-based) [12-16] are developed by fitting a preselected "waveform" to a suite of recorded regional ground motions. It should be acknowledged that deterministic (kinematic or dynamic) and hybrid source-based models also exist, offering a comprehensive platform for generating artificial ground motions, though at a very large computational cost [17]. Because of the latter characteristic such approaches, though powerful, are not widely utilized for comprehensive probabilistic seismic risk assessment. Stochastic models are preferred for this task with the record-based ones enjoying lately a wider appreciation by the structural engineering community [18] due to their versatility in selecting their waveform to capture all important features of ground motions, an advantage not necessarily shared by source-based models. For example, the most popular model within the latter category, the point-source model, cannot directly address spectral non-stationarities [11], an important excitation characteristic for inelastic structures –creating the so-called moving resonance [19].

This paper discusses the development of a record-based stochastic ground motion model for Chile utilizing a suite of ground motions recorded by the RENADIC (Red de cobertuta nacional de acelerografos) network and the Seismological Center of the University of Chile. A model that addressed both temporal and spectral non-stationarities is adopted, corresponding to a series of cascading single-degree-of-freedom (SDOF) oscillators with time-varying frequency and damping [12, 14]. The selection of these characteristics as well as of the characteristics of the temporal envelop function is then established in order to match the predominant waveforms in the available suite of ground motions. This leads to a complete parameterization of the stochastic ground motion model. An identification framework is then developed that provides the optimal fit of the parameterized model to a specific ground motion, and a validation of the resultant model is proposed in terms of the corresponding response spectrum. The results of this identification are then exploited to develop, though regression analyses, predictive relationships that relate the model parameters to seismicity characteristics (moment magnitude, rupture distance and soil classification). The corresponding model and regression relationships are finally validated by comparison to regional ground motion prediction equations [20].

2. Regional Characteristics and Seismological Database

Chile, located on the subduction zone between the Nazca Plate and the South American Plate, experiences significant seismic activity, including Some of the largest earthquakes ever-recorded (e.g. 1960 Valdivia and 2010 Maule seismic event) [21, 22]. Following the 2010 Maule earthquake, discussions have been initiated about modifying design practices, including placing greater emphasis on time-history analysis. The latter feature provides strong incentive for generating synthetic acceleration time histories, which is also aligns well with the objectives for this research endeavor.

The database used in this study is the one established by the National Seismological Center (CSN) and the National Network of Accelerograms (RENADIC) of the University of Chile. Details about the compilation of the entire database are included in [20, 23-25]. For the suite of ground motions used here, only subduction interplate events are examined. Though Chile is exposed to different types of earthquakes, such as interplate earthquakes, intraplate, outer rise and cortical earthquakes [25], most of the major earthquakes (representing the majority of the available recordings) correspond to an interplate mechanism. Describing all aforementioned type of earthquakes with a single stochastic model might be problematic, since their characteristics can be substantially different. Therefore the decision is made to focus the research effort ton interpolate events. In order to define such seismic events, only earthquakes characterized by a reverse faulting mechanism and epicenter location around the Chile-Peru trench with a depth between 20 and 55 km are considered.

Only large earthquakes and strong motion records were retained, corresponding to magnitudes over M_w 6.0 and peak ground acceleration (PGA) over 0.05g. As distance measure the rupture distance, as defined by Idini [25], is adopted, taking into account the rupture path and the shape of the contact between the plates. This option is considered more appropriate [26] than alternative measures for the subduction seismic events of the Chilean region [26]. Only records with rupture distance smaller then 250 km were retained.

All records are processed by a fourth order Butterworth filter whose [25]. The time-histories for a large number of the records in the database combined, along with the main seismic event, parts that appear to correspond to foreshocks and aftershocks (clearly distinguished by the main seismic event). To automatically identify the main seismic event the following procedure was adopted: using a moving window approach the envelope of the ground motion was determined (more details are provided in Section 4) and the main event was defined to correspond to the time window for which envelop remains within 1% of its peak value. Finally the records were classified according to the type of soil at the seismological station location. Since detailed soil classification information is not available, the generic classification proposed in [27] was used, distinguishing simply between rock or soil. The utilized database consisted of 33 events from 1985 to 2015, with magnitudes M_w ranging between 6.0 and 8.8 Mw and rupture distances R ranging between 30 km to 250 km. A total of 205 different records satisfied the previous assumptions, with 81 classified as rock and 124 as soil. Fig.1 shows the distribution for M and R of the events included in the database.

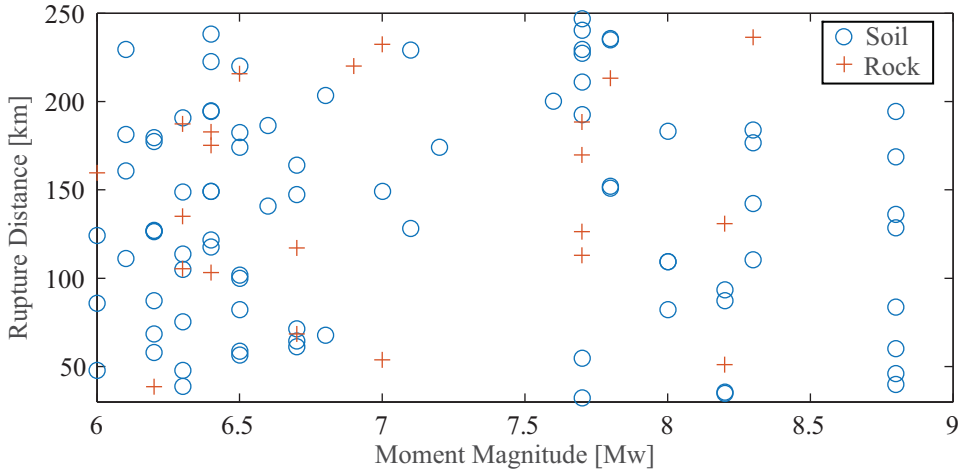

Fig. 1 – Distribution for moment magnitude and rupture distance for the seismic events used in this study.

3. Stochastic Ground Motion Model and its Parameterization

The stochastic ground motion model chosen addresses efficiently both temporal and spectral non-stationarities [7, 14]. The former is established through a time-domain modulating envelope function, whereas the latter is achieved by filtering a white-noise process using a filter corresponding to multiple cascading SDOF oscillators with time-varying characteristics. The discretized time series of the ground motion is modeled based on the suggestions in [12] as:

$$\ddot{a}(t\,|\,\boldsymbol{\theta},\mathbf{W}) = q(t\,|\,\boldsymbol{\theta}_e)\left[\sum_{i=1}^{k}\frac{h[t-t_i\,|\,\boldsymbol{\theta}_f(t_i))]}{\sqrt{\sum_{j=1}^{k}h[t-t_j\,|\,\boldsymbol{\theta}_f(t_j))]^2}}w(i\Delta t)\right] \quad k\Delta t < t < (k+1)\Delta t \tag{1}$$

where $\mathbf{W} = [w(i\Delta t) : i = 1,2,...,N_T]$ is the Guassian white-noise sequence, $\boldsymbol{\theta}$ is the vector of model parameters, distinguished between frequency $\boldsymbol{\theta}_f$ and time-domain $\boldsymbol{\theta}_e$ parameters, Δt is the chosen discretization interval (assumed here constant and equal to 0.005 s), $q(t\,|\,\boldsymbol{\theta}_e)$ is the time-modulating function, and $h[t-\tau\,|\,\boldsymbol{\theta}_f(\tau)]$ is an impulse response function corresponding to the pseudo-acceleration response of a linear SDOF oscillator with time varying frequency $\omega_f(\tau)$ and damping ratio $\zeta_f(\tau)$, in which τ denotes the time of the pulse

$$\begin{aligned} h[t-\tau\,|\,\boldsymbol{\theta}_f(\tau))] &= \frac{\omega_f(\tau)}{\sqrt{1-\zeta_f^2(\tau)}}\exp\left[-\omega_f(\tau)\zeta_f(\tau)(t-\tau)\right]\sin\left[\omega_f(\tau)\sqrt{1-\zeta_f^2(\tau)}(t-\tau)\right]; \quad \tau \le t \\ &= 0; \quad \text{otherwise} \end{aligned} \tag{2}$$

Note that the quantity in the brackets in (1) corresponds to a stochastic response with unit variance, meaning that the intensity characteristics of the ground motion are completely defined by the time envelope $q(t,\boldsymbol{\theta})$ [12].

For the time envelope modulating function the following expression, based on [28], is adopted

$$q(t\,|\,\boldsymbol{\theta}_e) = \begin{cases} a_1\left(\dfrac{t}{T_1}\right)^2 & \text{if } t > T_1 \\ a_1 & \text{if } T_1 \le t \le T_2 \\ a_1\exp\left[-a_2(t-T_2)^{a_3}\right] & \text{if } t > T_2 \end{cases} \tag{3}$$

where $\boldsymbol{\theta}_e$ is the model parameter vector for the temporal envelop (to be defined later). This envelop function was preferred over other candidates because it was found to provide a better match to the waveform characteristics of the available suite of ground motions [comparisons not reported here due to space limitations], and facilitate a balance between accuracy and complexity. It has a flat plateau (for time window [T_1 T_2]) with amplitude a_1, a quadratic rise up to time T_1, and an exponential decay after time T_2, with its shape defined by parameters a_2 and a_3. Mathematically this envelope is described by parameters [a_1 a_2 a_3 T_1 T_2]. This set of parameters can be related to physical properties of the excitation, and similarly to [12] concepts related to the Arias intensity are adopted here. The Arias intensity up to time t, $I_a(t)$, for the temporal envelope in Eq. (3) is given by:

$$I_a(t) = \frac{\pi}{2g}\int_0^t q^2(\tau\,|\,\boldsymbol{\theta}_e)d\tau \tag{4}$$

As properties of the excitation, to replace the mathematical parameter set {a_1 a_2 a_3} that have no clear physical interpretation, the total Arias intensity I_a [given by (4) for the total duration of excitation], the strong motion duration $D_{5\text{-}95}$ (defined as the duration for the Arias intensity to increase from 5% to 95% of its final value), and duration t_{50} corresponding to 50% of the Arias intensity, are used. For a chosen parameter set {T_1 T_2 $D_{5\text{-}95}$ t_{50}} parameters a_2 and a_3 are ultimately obtained through a solution of a nonlinear system of two equations so that parameter set {T_1 T_2 a_2 a_3} matches the target duration characteristics $D_{5\text{-}95}$ and t_{50}. Then a_1 can be

selected to match I_a. Therefore the model parameter vector for the temporal envelope is $\boldsymbol{\theta}_e$=[I_a T_1 T_2 $D_{5\text{-}95}$ t_{50}], with the first parameter scaling the amplitude of the envelope and the remaining ones modifying its shape.

For the time varying characteristics of the impulse response in Eq. (2), a linear variation is adopted for $\omega_f(\tau)$ and for the bandwidth [corresponding to the product of frequency and damping $\alpha_f(\tau)=\zeta_f(\tau)\omega_f(\tau)$]. These functional forms are similar, respectively, to the recommendations provided in [12] and [14], and were chosen here based on the time-varying frequency and bandwidth properties observed in the suite of ground motions in the database. The latter properties were obtained utilizing the moving window approach discussed in Section 4. A linear variation was then chosen as the best fit for the frequency and bandwidth characteristics. For the frequency the exponential decay suggested in [19] was also examined, but was found to provide similar level of accuracy, so the linear variation was ultimately preferred due to its simplicity. Fig. 2 demonstrates how the suggested functional forms are fitted to the characteristics for a recorded time history.

For the frequency the following parametric formulation is utilized

$$\omega_f(\tau)=\omega_p-(\omega_p-\omega_s)\frac{\tau-t_5}{t_{90}-t_5} \tag{5}$$

where t_{90} and t_5 correspond to the times 5% and 90%, respectively, of the Arias intensity is reached, and ω_p and ω_s are the corresponding reference frequencies, considered to correspond [14] to the frequencies for P and surface waves, respectively. The choice to use times t_{90} and t_5 as references (any two time instances could have used to describe the linear function for the frequency) is made so that the parametric description for the frequency variation is "anchored" to instances close to the beginning and end of the time-history, that also have a clear underlying physical interpretation (related to different types of seismic waves). The identification of the functional form of Eq. (5) (as described in the next section) for specific ground motions is based, through, to fit over the entire time-history, not just for these specific instances.

Similarly for the bandwidth we have

$$\alpha_f(\tau)=a_p-(a_p-a_s)\frac{\tau-t_5}{t_{90}-t_5} \tag{6}$$

where a_p and a_s are the reference values for the bandwidths associated with the P and surface waves, respectively. Therefore the model parameter vector for the impulse response function is $\boldsymbol{\theta}_f$=[ω_p ω_s a_p a_s].

Ultimately, the ground motion model has as parameters $\boldsymbol{\theta}$=[I_a T_1 T_2 $D_{5\text{-}95}$ t_{50} ω_p ω_s a_p a_s]. Following the recommendations in [12], the simulated time history is eventually high-pass filtered to guarantee a zero residual velocity. This filter corresponds to a critically damped oscillator with frequency 1 Hz and has a minimal impact on the response below this frequency.

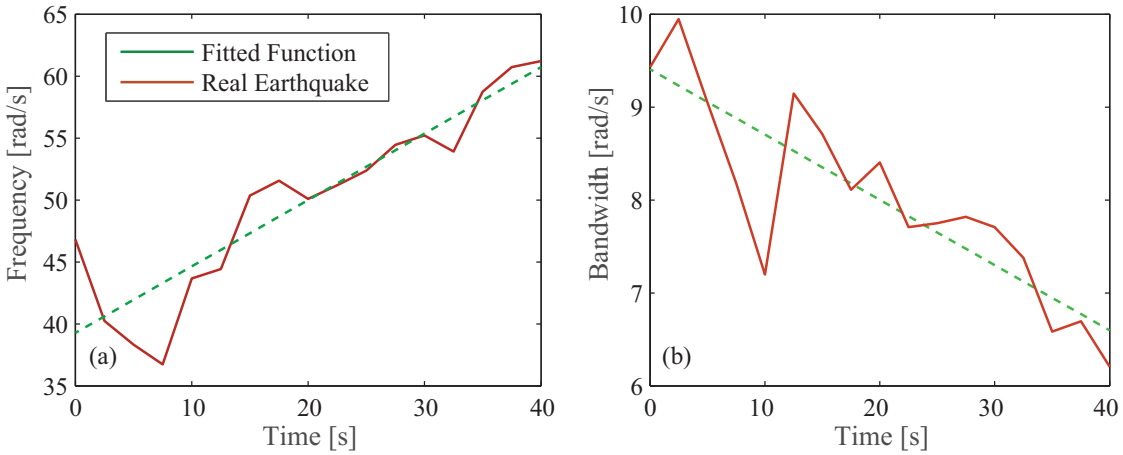

Fig. 2 – (a) Frequency and (b) bandwidth characteristics of a real ground motion and fitted functional variations.

4. Identification of Model Parameters

This section examines how $\boldsymbol{\theta}$ is chosen so that the stochastic ground motion model fits a specific time history $a_g(t)$. This is separately performed for the temporal envelope and the frequency filter parameters. The process has as foundation the determination of the characteristics within a moving window of short duration, as suggested in [14]. This process is reviewed first here.

4.1 Moving Time-Window

The moving time-window approach analyzes the non-stationarity of the accelerogram $a_g(t)$ assuming that for a short period ΔT this accelerogram can be approximated as stationary process. This allows a stationary auto-regressive (AR) model to be fitted to successive segments of $a_g(t)$ and obtain information about $\boldsymbol{\theta}$. Each segment is centered at time t_m (so extends from t_m-$\Delta T/2$ to t_m+$\Delta T/2$) and ultimately supports (see discussion next) the identification of the most probable AR model for that segment, whose characteristics are then attributed to time-instance t_m. Moving t_m along the record using some time step Δt_s the time-varying characteristics of $a_g(t)$ are obtained. For the second-order model representing the frequency variation [corresponding to the impulse function of Eq. (2)], the parameters of the equivalent second-order AR model are given by the least squares solution $\hat{\mathbf{a}}_p(t_m) = (\mathbf{Y}^T\mathbf{Y})^{-1}\mathbf{Y}^T\mathbf{y}$ [14] where, assuming that $a_g(t)$ is provided with a constant time strep Δt_g, the observation matrix and output vector are, respectively

$$\mathbf{y}^T = \begin{bmatrix} a_g(t_m^3) & a_g(t_m^4) & \dots & a_g(t_m^N) \end{bmatrix},\ \mathbf{Y}^T = \begin{bmatrix} a_g(t_m^2) & a_g(t_m^3) & \dots & a_g(t_m^{N-1}) \\ a_g(t_m^1) & a_g(t_m^2) & \dots & a_g(t_m^{N-2}) \end{bmatrix} \tag{7}$$

with $a_g(t_m^i)$ representing the accelerogram value at the i^{th} time instance within time-window [t_m-$\Delta T/2$, t_m+$\Delta T/2$] and N representing the total number of time steps it this window. The relationship between $\hat{\mathbf{a}}_p(t_m)$ and the frequency and damping (or bandwidth) of the second order model may be then obtained by matching free vibration solutions as [14]

$$\begin{aligned} \hat{a}_1(t_m) &= 2\,\mathrm{e}^{-\omega(t_m)\zeta(t_m)\Delta t_g}\cos(\omega(t_m)\sqrt{1-\zeta^2(t_m)}\Delta t_g) \\ \hat{a}_2(t_m) &= -\mathrm{e}^{-2\omega(t_m)\zeta(t_m)\Delta t_g} \end{aligned} \tag{8}$$

Identificaiton of the frequency and damping completely defines he characteristics of the impulse function (2), since its amplitude is not required (normalized to unit variance based on the adopted here formulation).

The envelope value of the accelerogram can be also obtained by looking at the RMS value within the time window

$$e(t_m) = \sqrt{\frac{1}{N}\sum_{i=1}^{N} a_g^2(t_m^i)} \tag{9}$$

4.2 Identification of temporal envelope characteristics

For identifying the temporal envelop characteristics the fit to the arias intensity variation has been suggested in the literature [7]. For the time-history $a_g(t)$ the Arias intensity up to time t is given by

$$I_g(t) = \frac{\pi}{2g}\int_0^t a_g^2(\tau)d\tau \tag{10}$$

then $\boldsymbol{\theta}_g$ can be selected so that the difference between $I_g(t)$ (for the actual accelerogram) and $I_\alpha(t)$ given by (4) (for the temporal envelop) is minimized. This approach corresponds to a fit to cumulative characteristics of the time envelop up to each time instance, which might not necessarily provide a good fit based on instantaneous variation for the envelop characteristics. To address this shortcoming and exploiting the moving time-window concept discussed in the previous section, an alternative objective is introduced in this work, corresponding to a direct comparison of $q(t|\boldsymbol{\theta}_e)$ and the envelope value for the accelerogram $e(t_m)$ given by Eq. (9). This ultimately leads to the following optimization problem for identifying $\boldsymbol{\theta}_e$

$$\boldsymbol{\theta}_e = \arg\min\left(f_{e1}(\boldsymbol{\theta}_e) + \gamma_e f_{e2}(\boldsymbol{\theta}_e)\right)$$
$$f_{e1}(\boldsymbol{\theta}_e) = \frac{\sum_{i=1}^{N_t}\left(I_g(t^i) - I_a(t^i)\right)^2}{\sum_{i=1}^{N_t} I_g(t^i)^2} \;\; ; \;\; f_{e2}(\boldsymbol{\theta}_e) = \frac{\sum_{i=1}^{N_t}\left(e_g(t^i) - q(t^i \mid \boldsymbol{\theta}_e)\right)^2}{\sum_{i=1}^{N_t} e_g(t^i)^2} \tag{11}$$

where f_{e1} and f_{e2} represent the aforementioned two objectives (appropriately normalized through the quantities appearing in the denominator), γ_e is a weighting function, t^i is the i^{th} time instance used in the evaluation of the objectives and N_t is the total number of time instances used in this evaluation. It was found that using the combined objectives provided better fit across the entire database than using one of them. Fig. 3 demonstrates key comparisons; it shows the characteristics (intensity, envelope) for a time history $a_g(t)$ as well as the corresponding ones for the fitted envelope based on the combined objectives f_{e1} and f_{e2} and for only objective f_{e1}. It is evident that, at least in this case, the optimization using the combined objectives leads to a much better fit to the envelope of the strong ground motion, providing a further justification for the proposed modification for the temporal envelope fit.

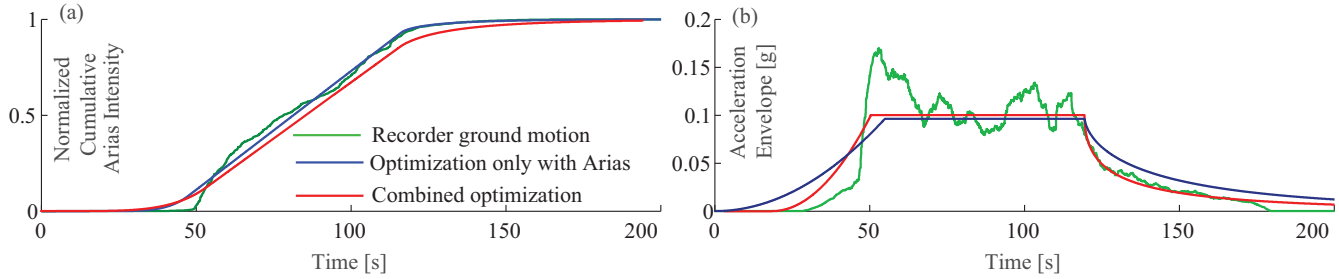

Fig. 3 – Demonstration of the temporal envelope fit over a real ground motion using different approaches for (a) cumulative Arias intensity and (b) acceleration envelope

4.3 Identification of frequency characteristics

For the frequency characteristics $\boldsymbol{\theta}_f$, the identification is performed by minimizing the discrepancy between the frequency and bandwidth functions given, respectively, by (5) and (6) and the frequency and bandwith identified by the moving time-window approach given by (8). This identification is performed through the minimization

$$\{\omega_p \;\; \omega_s\} = \arg\min \frac{1}{N_t}\sum_{i=1}^{N_t}\left(\omega_f(t^i) - \omega(t^i)\right)^2$$
$$\{a_p \;\; a_s\} = \arg\min \frac{1}{N_t}\sum_{i=1}^{N_t}\left(a_f(t^i) - a(t^i)\right)^2 \tag{12}$$

where t^i is the i^{th} time instance used in the evaluation and N_t is the total number of time instances used.

4.4 Identification over the entire database and validation of the fitted ground motion model

The approach discussed in Sections 4.2 and 4.3 is implemented now over the entire database of strong ground motions. The numerical characteristics chosen are: ΔT= 5 s duration of the moving time-window with Δt_s= 0.75 s step, optimizations of Eqs. (11) and (12) are performed for all instances resulting from this time step, and selection of weight γ_e is equal to 0.5. The identified stochastic ground motion model is then validated by comparing the resulting spectrum for a 5% damped SDOF oscillator. Fig. 4 shows this comparison for a specific case. The spectrum for 100 synthetic ground motions, as well as the median is shown. The comparison is performed by comparing that median to the spectrum of the recorded ground motion.

The comparison is then extended over the entire database. Two different error measures are calculated, mean relative error, calculated over all periods, and peak relative-error (error for the peak of the response spectrum). The statistics are, respectively, 15% and 35%, which show a good overall fit.

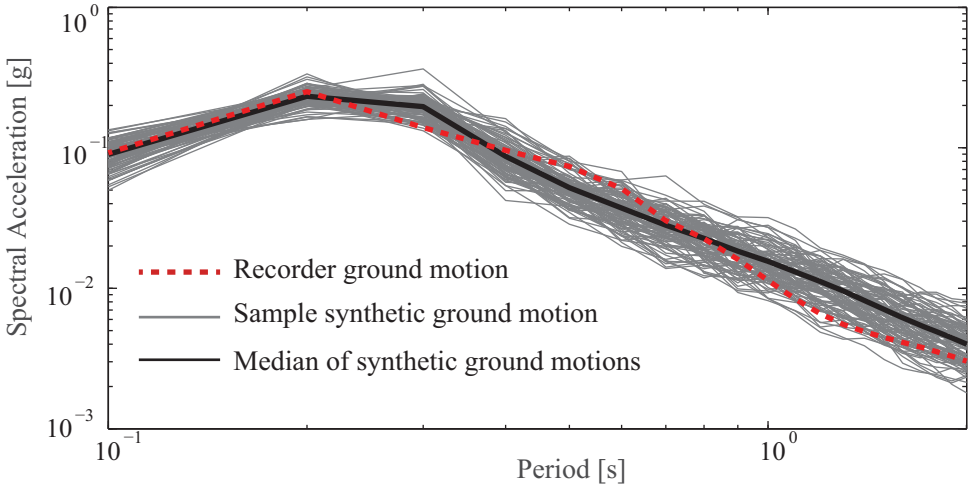

Fig. 4 – Comparison between response spectra for a recorded ground motion and the synthetic ground motions provided by the fitted stochastic ground motion model.

5. Predictive Relationships for the Ground Motion Model Parameters

With a validated model that has been fitted over the entire database, the next step is to establish the predictive relationships that connect the model parameters $\boldsymbol{\theta}$ to the seismological characteristics that describe the database, the moment magnitude M and the rupture distance R. This is established through a regression analysis, which is performed here separately for records classified as rock or soil. The regression analysis here is established for the horizontal component corresponding to the largest value of the Arias intensity (strong ground motion component). Different regression functions were considered for the Chilean subduction zone with the final selection made based on similar functional forms available in the literature [29, 30] and the existing attenuation curves for Chile [20, 23]. The selected functional forms for the model parameter vector $\boldsymbol{\theta}$=[I_a T_1 T_2 $D_{5\text{-}95}$ t_{50} ω_p ω_s a_p a_s] are

$$\begin{aligned}
\log(\theta_i) &= c_{1i} + (c_{2i}M + c_{3i})\log(R+10) + c_{4i}M + c_{5i}(R+10) && i=1\ \{I_a\} \\
\log(\theta_i) &= c_{1i} + c_{2i}\log(M) + c_{3i}\log(R) && i=2,3\ \{T_1\ T_2\} \\
\log(\theta_i) &= c_{1i} + c_{2i}\log(M) + c_{3i}\log(R) + c_{4i}M && i=4\ \{D_{5-95}\} \\
\log(\theta_i) &= c_{1i} + c_{2i}\log(M) + c_{3i}\log(R) + c_{4i}M + c_{5i}M^2 && i=5\ \{t_{50}\} \\
\theta_i &= c_{1i} + c_{2i}\log(M) + c_{3i}\log(R) && i=6,7,8,9\ \{\omega_p\ \omega_s\ a_p\ a_s\}
\end{aligned} \tag{13}$$

The regression is performed through a standard maximum likelihood approach, with the regression residuals decomposed in intraevent and interevent following the methodology in [31]. The optimized coefficients and normalized residual variances [separated into intraevent (τ^2) and interevent (σ^2)] are reported in Table1. Normalization is established with respect to the variance for the data γ^2 (also shown in Table 1). In Table 2 the correlation of the residuals is reported. Fig. 5 plots also the residuals for some specific cases of interest.

Based on the regression results the generation of a synthetic ground motion for a specific seismological scenario follows the following steps:

1) Given seismological parameters M and R the mean value for the ground motion model parameters $\overline{\theta}_i$ is obtained through regression relationships in Eq. (13), using the optimized coefficients from Table 1. This defines the mean vector $\overline{\boldsymbol{\theta}}$.
2) A random sample is generated for the residuals for $\boldsymbol{\theta}$ from a Gaussian distribution with zero mean, and covariance matrix with variance $\gamma^2(\tau^2+\sigma^2)$ as reported in Table 1 and correlation coefficients the ones in Table 2. This defines the residual vector $\tilde{\boldsymbol{\theta}}$.
3) The model parameter vector is given by combining the previous two components $\boldsymbol{\theta} = \overline{\boldsymbol{\theta}} + \tilde{\boldsymbol{\theta}}$. If the preference is to use the mean regression predictions only, the second component should be ignored.

4) A white noise sequence is generated $\mathbf{W} = [w(i\Delta t) : i = 1, 2, ..., N_T]$ and a synthetic ground motion is obtained through Eq. (1). This further entails identification of parameters a_1 and a_2 based on values $\{T_1\ T_2\ D_{5\text{-}95}\ t_{50}\}$, as described in Section 3.

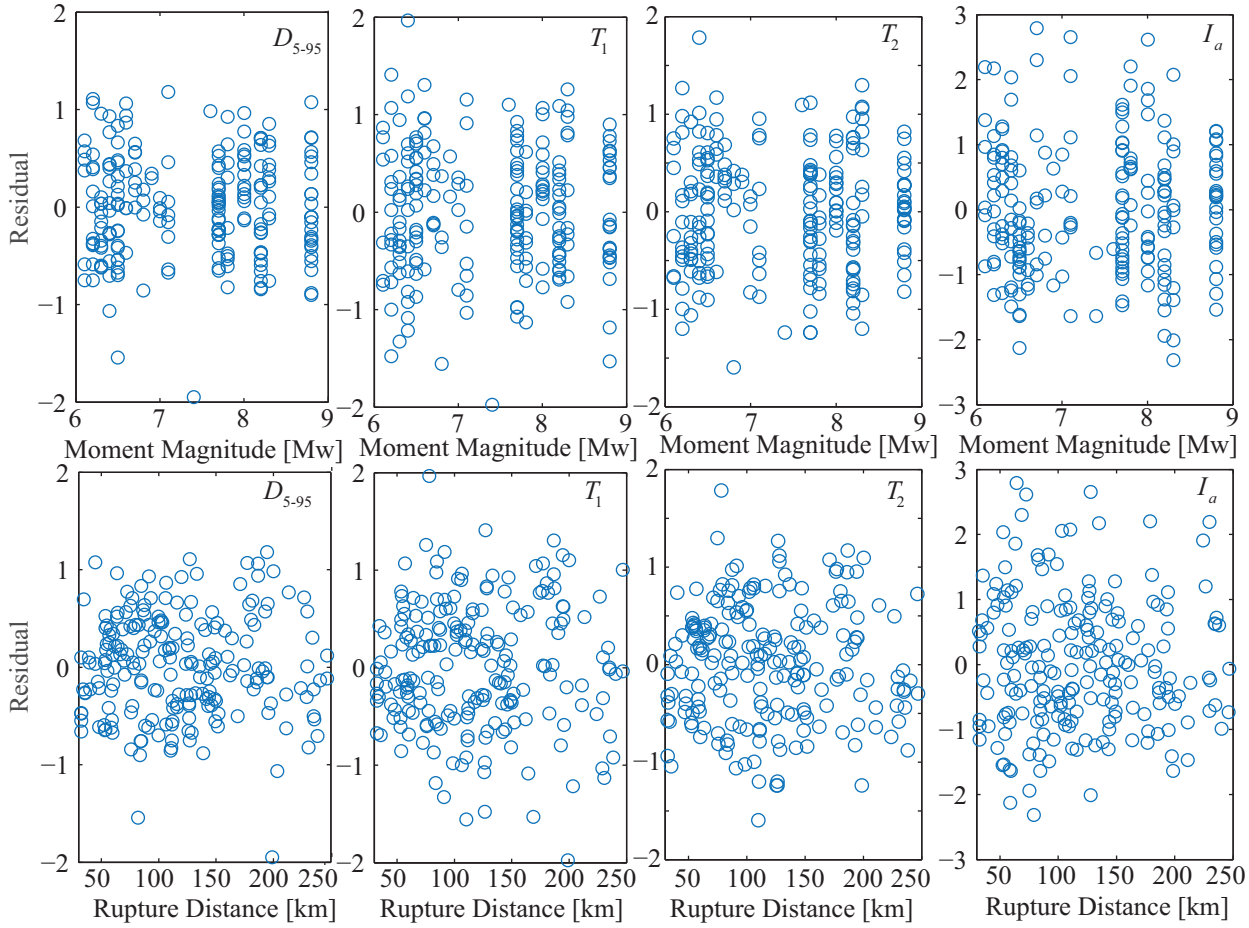

Fig. 5 – Residuals for the regression relationships as function of M and R for soil classification for different model parameters (denoted at the right top corner in each plot).

Table 1: Optimized coefficients for records simulated on Rock and Soil (in parenthesis) sites. Units in this Table correspond to s for T_1, T_2, t_{50}, $D_{5\text{-}95}$, rad/s for ω_p, ω_s, α_p, α_s, and g^2 for $I_a 2g/\pi$.

Par.	c_1	c_2	c_3	c_4	c_5	σ^2	τ^2	γ^2
$I_a 2g/\pi$	-49.68 (-24.95)	-1.05 (-0.37)	8.54 (2.42)	6.00 (3.22)	-0.02 (-0.01	0.38 (0.16)	0.10 (0.10)	3.11 (2.82)
T_1	-5.23 (-5.18)	3.42 (3.66)	0.24 (0.11)	0 (0)	0 (0)	0.71 (0.67)	0.06 (0.07)	0.59 (0.65)
T_2	-6.42 (-6.04)	4.33 (4.30)	0.16 (0.08)	0 (0)	0 (0)	0.56 (0.52)	0.10 (0.08)	0.58(0.76)
t_{50}	-16.46 (-9.01)	13.46 (14.47)	0.14 (0.05)	-0.93 (-3.31)	-0.02 (0.13)	0.54 (0.43)	0.10 (0.11)	0.59 (0.61)
$D_{5\text{-}95}$	-18.77 (6.23)	16.31 (-8.88)	-0.11 (-0.24)	-1.55 (1.96)	0 (0)	0.44 (0.34)	0.03 (0.02)	0.67 (0.76)
ω_p	11.98 (86.02)	16.56 (-16.85)	-2.71 (-4.21)	0 (0)	0 (0)	0.82 (0.78)	0.10 (0.11)	0.90 (0.88)
ω_s	8.79 (78.38)	18.80 (-10.58)	-2.98 (-5.50)	0 (0)	0 (0)	0.80 (0.72)	0.09 (0.15)	0.95 (0.96)
α_p	2.15 (3.09)	0.08 (0.16)	-0.12 (-0.40)	0 (0)	0 (0)	0.77 (0.75)	0.13 (0.14)	0.78 (0.65)
α_s	3.39 (3.94)	-0.77 (-0.86)	-0.04 (-0.16)	0 (0)	0 (0)	0.71 (0.87)	0.20 (0.02)	0.91 (0.90)

Table 2: Correlation coefficients of residuals for records simulated on Rock and Soil (in parenthesis) sites

Par.	I_a	T_1	T_2	D_{50}	$D_{5\text{-}95}$	ω_p	ω_s	α_p	α_s
I_a	1	0.26 (0.26)	0.47 (0.34)	0.43 (0.37)	0.70 (0.65)	0.29 (0.04)	0.16 (-0.05)	0.01 (-0.01)	0.18 (0.10)
T_1		1	0.77 (0.89)	0.90 (0.94)	0.53 (0.52)	0.12 (0.01)	-0.09 (0.04)	0.03 (0.05)	0.11 (0.06)
T_2			1	0.94 (0.98)	0.77 (0.67)	0.02 (-0.01)	-0.15 (-0.06)	0.18 (0.01)	0.05 (0.03)
D_{50}				1	0.76 (0.68)	0.06 (-0.01)	-0.14 (-0.03)	0.22 (0.03)	0.08 (0.04)
$D_{5\text{-}95}$					1	0.21 (-0.08)	0.02 (-0.17)	-0.01(-0.05)	0.18 (0.01)
ω_p			symmetric			1	0.78 (0.62)	0.28(0.13)	0.63 (0.60)
ω_s							1	0.30 (0.44)	0.28 (0.48)
α_p								1	0.38(0.41)
α_s									1

6. Preliminary Validation against Regional Ground Motion Prediction Equations

The stochastic ground motion model is finally validated against the ground motion prediction equations (GMPEs) –also referenced as attenuation relationships– available for Chile [20]. Synthetic ground motions are obtained through the process described in Section 5 and their spectrum is averaged over 100 samples. These median predictions are then compared to the GMPE by Boroschek and Contreras [20] for a reference focal depth of H=30 km. Results are reported in Fig. 6 for earthquakes for soil classification. Since the GMPEs in [20] refer to the median horizontal component of the ground motions and the predictive relationships were developed here for the strong component (research team is currently developing relationships for the median as well), the following modification is established for a consistent comparison: a correction factor is developed and the results from the stochastic ground motion model are adjusted by this factor. This correction factor is established through the following process: for each ground motion in the database the square root of the ratio of the arias intensity between the median horizontal component and the strongest horizontal component is calculated, and then a regression relationship is developed for this ration. This relationship, found to be 0.8+0.05log(M)-0.017log(R), represents the desired correction factor. The results in Fig. 6 show overall a good agreement, but also for some scenarios (smaller rupture distances) larger discrepancies, that partially contradicts the validation against the database discussed in Section 4.4. This can be potentially attributed to the approximation established here for correcting the predictions to the median ground motion component (comparison will be updated as soon as the new regressions are developed). A potential remedy for these discrepancies would be to enhance the current approach for optimizing the regression characteristics with the approach advocated in [32] that can facilitate a direct match to any GMPE.

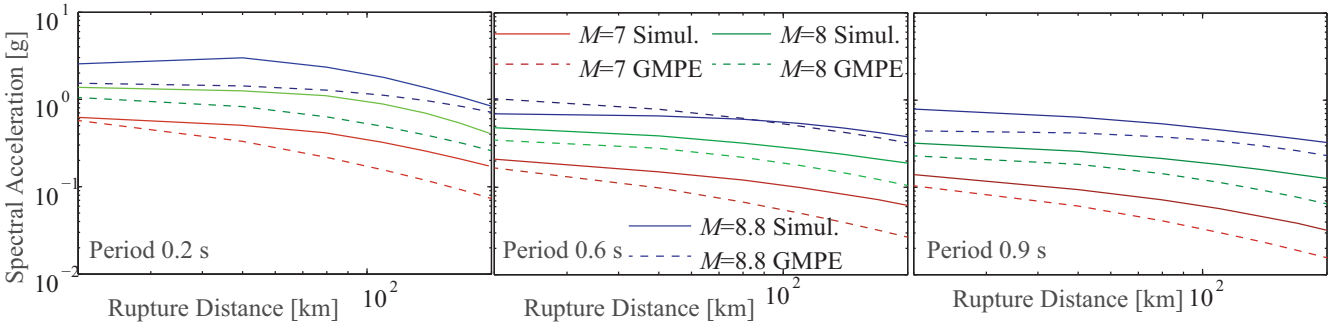

Fig. 6 – Comparison of results of stochastic ground motion model (Simul. in the figurelegend) to a regional GMPE for 5% damped SDOFs with different natural periods [0.2, 0.6 and 0.9 s].

7. Conclusions

The development of a record-based stochastic ground motion model for the Chilean subduction region was discussed in this paper, utilizing a database provided by the RENADIC and CSN networks that considers [25] thrust earthquakes along the Chile-Peru trench of magnitudes over 6.0 and within 250 km of the source. A widely used stochastic model that addresses both temporal and spectral non-stationarities was adopted, corresponding to a series of cascading SDOF oscillators with time-varying frequency and bandwidth characteristics. An identification framework is then developed that provides the optimal fit of the parameterized model to a specific ground motion, using a moving time-window approach for identifying the time-varying characteristics of recorded ground motions. For the fitted stochastic ground motion model, linear variation for the frequency and bandwidth were proposed, as this was found to match well the trends in the available database. A temporal envelop that combines a quadratic growth, a plateau and an exponential decay was adopted, and its fit was establish in order to match both the energy and peak characteristics of the recorded ground motions. Validation of the resultant model in terms of the corresponding spectrum (comparing original ground motion and fitted stochastic ground motion model) showed good agreement. A regression analysis was then established to connect the parameters of the stochastic ground motion model to seismological characteristics (moment magnitude and rupture distance). This provides the ability to create synthetic ground motions for different seismological scenarios. The developed model was finally validated by comparison to regional ground motion prediction equations. Discrepancies that were reported are a topic of current investigation by the research team.

8. Acknowledgments

The ground motion data for this work were provided by RENADIC and the National Seismological Center at University of Chile. This is gratefully appreciated by all authors. The first author would also like to acknowledge support from CONICYT through a program entitled “Estadias Cortas en el Extranjero para estudiantes de Ingeniería Civil”.

9. References

[1] Goulet CA, Haselton CB, Mitrani-Reiser J, Beck JL, Deierlein G, Porter KA, Stewart JP (2007) Evaluation of the seismic performance of code-conforming reinforced-concrete frame building-From seismic hazard to collapse safety and economic losses. *Earthquake Engineering and Structural Dynamics,* **36** (13), 1973-1997.

[2] Taflanidis AA, Beck JL (2009) Life-cycle cost optimal design of passive dissipative devices. *Structural Safety,* **31** (6), 508-522.

[3] Lin T, Haselton CB, Baker JW (2013) Conditional spectrum-based ground motion selection. Part I: Hazard consistency for risk-based assessments. *Earthquake Engineering and Structural Dynamics,* **42** (12), 1847-1865.

[4] Jalayer F, Beck JL (2008) Effects of two alternative representations of ground-motion uncertainty in probabilistic seismic demand assessment of structures. *Earthquake Engineering and Structural Dynamics,* **37** (1), 61-79.

[5] Grigoriu M (2011) To scale or not to scale seismic ground-acceleration records. *Journal of Engineering Mechanics, ASCE,* **137** (4), 284-293.

[6] Radu A, Grigoriu M (2014): A comparative study on fragility analyses in earthquake engineering. *9th International Conference on Structural Dynamics, EURODYN 2014*, 30 June - 2 July Porto, Portugal.

[7] Rezaeian S, Der Kiureghian A (2010) Simulation of synthetic ground motions for specified earthquake and site characteristics. *Earthquake Engineering & Structural Dynamics,* **39** (10), 1155-1180.

[8] Atkinson GM, Silva W (2000) Stochastic modeling of California ground motions. *Bulletin of the Seismological Society of America,* **90** (2), 255-274.

[9] Au SK, Beck JL (2003) Subset simulation and its applications to seismic risk based on dynamic analysis. *Journal of Engineering Mechanics, ASCE,* **129** (8), 901-917.

[10] Gidaris I, Taflanidis AA (2015) Performance assessment and optimization of fluid viscous dampers through life-cycle cost criteria and comparison to alternative design approaches. *Bulletin of Earthquake Engineering,* **13** (4), 1003-1028.

[11] Boore DM (2003) Simulation of ground motion using the stochastic method. *Pure and Applied Geophysics,* **160**, 635-676.

[12] Rezaeian S, Der Kiureghian A (2008) A stochastic ground motion model with separable temporal and spectral nonstationatiries. *Earthquake Engineering and Structural Dynamics,* **37**, 1565-1584.

[13] Conte JP, Peng BF (1997) Fully nonstationary analytical earthquake ground-motion model. *Journal of Engineering Mechanics, ASCE,* **12**, 15-34.

[14] Papadimitriou K (1990): *Stochastic characterization of strong ground motion and application to structural response*. Pasadena, CA. *Report No. EERL 90-03*, California Institute of Technology.

[15] Dickinson BW, Gavin HP (2011) A parametric statistical generalization of uniform hazard earthquake ground motions. *Journal of Structural Engineering, ASCE,* **137** (3), 410-422.

[16] Vlachos C, Papakonstantinou KG, Deodatis G (2016) A multi-modal analytical non-stationary spectral model for characterization and stochastic simulation of earthquake ground motions. *Soil Dynamics and Earthquake Engineering,* **80**, 177-191.

[17] Bao H, Bielak J, Ghattas O, Kallivokas LF, O'Hallaron DR, Shewchuk JR, Xu J (1998) Large-scale simulation of elastic wave propagation in heterogeneous media on parallel computers. *Computer Methods in Applied Mechanics and Engineering,* **152** (1-2), 85-102.

[18] Vetter C, Taflanidis A (2014) Comparison of alternative stochastic ground motion models for seismic risk characterization. *Soil Dynamics and Earthquake Engineering,* **58**, 48-65.

[19] Beck JL, Papadimitriou C (1993) Moving resonance in nonlinear response to fully nonstationary stochastic ground motion. *Probabilistic Engineering Mechanics,* **8** (3-4), 157-167.

[20] Boroschek R, Contreras V (2012): Strong ground motion form the 2010 Mw 8.8 Maule Chile earthquake and attenuation relations for Chilean subduction zone interface earthquakes. *International Symposium on Engineering Lessons Learned from the 2011 Great East Japan earthquake*, March 1-4 Tokyo, Japan.

[21] Lomnitz C (2004) Major earthquakes of Chile: a historical survey, 1535-1960. *Seismological Research Letters,* **75** (3), 368-378.

[22] Elnashai AS, Gencturk B, Kwon O-S, Al-Qadi IL, Hashash Y, Roesler JR, Kim SJ, Jeong S-H, Dukes J, Valdivia A (2010): *The Maule (Chile) earthquake of February 27, 2010: Consequence assessment and case studies*. MAE Center Report No. 10-04.

[23] Ruiz S, Saragoni RG (2005): Fórmulas de Atenuación para la Subducción de Chile Considerando los dos Mecanismos de Sismogénesis y los Efectos del Suelo. *Congreso Chileno de Sismología e Ingeniería Antisísmica IX Jornadas*.

[24] Boroschek RL, Contreras V, Kwak DY, Stewart JP (2012) Strong ground motion attributes of the 2010 Mw 8.8 Maule, Chile, earthquake. *Earthquake Spectra,* **28** (S1), S19-S38.

[25] Idini B (2016): *Curvas de atenuación para terremotos intraplaca e interplaca en la zona de subducción chilena, Tesis para optar al grado de Magíster en Ciencias de la Ingeniería, mención en Ingeniería Sísmica.* Universidad de Chile, Santiago, Chile.

[26] Moreno M, Rosenau M, Oncken O (2010) 2010 Maule earthquake slip correlates with pre-seismic locking of Andean subduction zone. *Nature,* **467** (7312), 198-202.

[27] Contreras V, Boroschek R (2012): Strong ground motion attenuation relations for Chilean subduction zone interface earthquakes. *Proceedings of 15th world conference on earthquake engineering (15WCEE)* Lisbon, Portugal.

[28] Housner GW, Jennings PC (1964) Generation of artificial earthquakes. *Journal of the Engineering Mechanics Division,* **90** (1), 113-152.

[29] Atkinson GM, Boore DM (2003) Empirical ground-motion relations for subduction-zone earthquakes and their application to Cascadia and other regions. *Bulletin of the Seismological Society of America,* **93** (4), 1703-1729.

[30] Zhao JX, Zhang J, Asano A, Ohno Y, Oouchi T, Takahashi T, Ogawa H, Irikura K, Thio HK, Somerville PG (2006) Attenuation relations of strong ground motion in Japan using site classification based on predominant period. *Bulletin of the Seismological Society of America,* **96** (3), 898-913.

[31] Abrahamson NA, Youngs RR (1992) A stable algorithm for regression analyses using the random effects model. *Bulletin of the Seismological Society of America,* **82** (1), 505-510.

[32] Vetter C, Taflanidis AA, Mavroeidis GP (2016) Tuning of stochastic ground motion models for compatibility with ground motion prediction equations. *Earthquake Engineering and Structural Dynamics,* **45** (6), 893-912.